Published in final edited form as:
IEEE Trans Ultrason Ferroelectr Freq Control. 2015 February ; 62(2): 337–349. doi:10.1109/TUFFC.2014.006784.

Intracardiac Myocardial Elastography in canines and humans *in vivo*

Julien Grondin[1], **Elaine Wan**[2], **Alok Gambhir**[2], **Hasan Garan**[2], and **Elisa E. Konofagou**[1,3]

[1]Department of Biomedical Engineering, Columbia University, New York, USA

[2]Department of Medicine, Columbia University, New York, USA

[3]Department of Radiology, Columbia University, New York, USA

Abstract

Intracardiac echocardiography (ICE) is a useful imaging modality which is used during radiofrequency (RF) ablation procedures to help identify anatomical structures. Utilizing ICE in adjunct with myocardial elastography (ME) can provide additional information on the mechanical properties of cardiac tissue and provide information on mechanical changes due to ablation. The objective of this study was to demonstrate that ICE can be used at high frame rate using a diverging beam transmit sequence to image myocardial strain and differentiate myocardial tissue properties before, during and after ablation for a clinical ablation procedure. In this feasibility study, three normal canines and eight patients with atrial fibrillation (AF) were studied *in vivo*. A 5.8-MHz ICE transducer was used to image the heart with a diverging beam transmit method achieving 1200 frames per second (fps). Cumulative axial displacement estimation was performed using 1-D cross-correlation with a window size of 2.7mm and 95% overlap. Axial cumulative strains were estimated in left atrium (LA) and right atrium (RA) using a least-squares estimator with a kernel of 2mm on the axial displacements.

In the canine case, radial thickening was detected in the lateral wall and in the interatrial septum during LA emptying. For AF patients, mean absolute strain in the ablated region was lower (6.7±3.1%) than before the ablation (17.4±9.3%) in LA at end LA emptying. In the cavotricuspid isthmus (CTI) region, mean absolute strain magnitude at end RA emptying was found to be higher during ablation (43.0±18.1%) compared to after ablation (33.7±15.8%). Myocardial strains in the LA of an AF patient were approximately 2.6 times lower in the ablated region than before ablation. This initial feasibility may suggest ME as a new imaging modality to be used in adjunct with ICE in RF ablation guidance and lesion monitoring.

Keywords

Intracardiac echocardiography; myocardial elastography; Radiofrequency ablation; Lesion characterization; high frame rate imaging

ek2191@columbia.edu.

INTRODUCTION

A. Radiofrequency ablation of atrial fibrillation

Atrial fibrillation (AF) is a disorder of heart rhythm that is estimated to affect 2.3-5.1 million people in the US and is expected to involve more than 5.6-12.1 million by 2050 [1, 2]. Radiofrequency (RF) ablation can be used to treat AF. The procedure requires percutaneous insertion of catheters into the heart and application of alternating electrical current on arrhythmogenic regions of the myocardium to generate lesions [3]; such as electrical isolation of the pulmonary veins. Being able to identify and characterize lesion gaps, as well as, transmurality of lesions is of paramount interest to improve the success rate of ablation procedures and decrease the need for repeat ablations [4-6]. Determinants of lesion transmurality include contact force applied by the catheter on the myocardium [7], impedance [8], power, temperature [9] and duration of ablation [10]. However, there are currently no technologies clinically available that allow for real time assessment of tissue changes due to RF delivery. Ultrasound techniques such as contrast-enhanced ultrasound [11, 12] or elastography [13] have also been considered to monitor ablation lesions but has been mainly applied to kidney or liver and used externally placed ultrasound probes which can not easily be integrated in a clinical cardiac ablation setting.

B. Intracardiac echocardiography during radiofrequency ablation

Intracardiac echocardiography (ICE) is commonly used to provide real-time imaging of the heart to identify anatomic structures and guide RF ablation. Using ICE as an imaging modality for lesion characterization would forego the need for additional equipment or modification of the ablation procedure or clinical setup.

ICE has been previously used to characterize endocardial lesions based upon tissue swelling and increase in tissue echogenicity [3, 14]. However, this technique tends to overestimate the lesion size and its efficiency remains to be proven. In addition, echogenicity does not provide quantitative or qualitative information about the mechanical characteristics of the tissue and its changes during RF delivery. Although tissue temperature can indicate tissue desiccation and denaturation of tissue proteins [15], which can result in an increase in elastic modulus of tissues [16, 17], catheters currently used for RF ablation are irrigated tip catheters which provide catheter tip temperature, but do not provide direct tissue temperature measurements. None of the current feedback information such as temperature, power, impedance and ablation duration, provide information on tissue stiffness or contractility which decreases during ablation. Previous studies have reported a decrease in atrial strain or strain-related parameters in humans [18] and canines [19] who received RF ablation six month prior.

C. Intracardiac echocardiography for myocardial tissue mechanics assessment

ICE has been used in the past in the field of cardiac motion estimation. Wang et al. have assessed strains in the anterior region of the myocardium in a canine model using M-mode Tissue Doppler Imaging (TDI) [20]. However, this method required a compromise between the frame rate and the field of view of the heart and only a specific region of the myocardium was investigated. Another previous study, assessed strain rate from M-mode

tissue velocity from ICE imaging in the porcine model [21], but this study presented similar shortcomings as the previous one. Yue et al. have assessed myocardial strain in a canine model using speckle tracking on B-mode images [22]. This method suffered nevertheless both from the loss of phase information due to envelope detection and from a low frame rate (30 fps) which affected the quality of motion estimation. More recently, acoustic radiation force impulse (ARFI) has been applied to ICE to characterize myocardial stiffness by measuring shear wave velocity [23]. ARFI has also been used with ICE to assess RF ablation lesions in canine and porcine [24, 25]. However these studies used a depth of field below 3 cm which required the ICE catheter to be close to the surface of the myocardium and did not allow for a full clinical imaging window and moreover, the study was limited to animals.

Herein we present a study in humans which using Myocardial Elastography (ME) in adjunct with ICE allows for assessment of the mechanical properties of the myocardium, a surrogate marker of electrical conduction, and thus can be used to characterize the extension and efficacy of ablation lesions. It has recently been reported that LA strain can predict the success of AF ablation [26-28]. Previous studies have shown that strains could be obtained with ME at a high frame rate and a large field of view of the heart [29]. High frame rate ultrasound imaging can be achieved with techniques such as composite imaging [30] or parallel beamforming using plane wave [31] or diverging beams [32, 33]. Diverging beams have the advantage of reconstructing a large field of view at a very high frame rate. To the authors knowledge, high frame rate imaging using diverging beams has never been used with ICE. In this study, our objective was (1) to use diverging wave imaging and parallel beamforming with ICE to image myocardial strain at high temporal resolution during atrial emptying in canines and humans *in vivo* and (2) to demonstrate that strain imaging with ICE can differentiate myocardial tissue properties before, during and after ablation for a clinical ablation procedure.

METHODS

A. Canine study

A preliminary feasibility study was performed in the canine model. Three male canines ranging from 23 to 25 kg in weight were premedicated with diazepam 0.5-1.0 mg/kg injected intravenously and then anesthetized with an intravenous injection of propofol 2-5 mg/kg. The canines were mechanically ventilated with a rate- and volume-regulated ventilator on a mixture of oxygen and titrated 0.5-5.0 % isoflurane. An ICE catheter was inserted into the jugular vein through a 10 F introducer sheath and advanced to the right atrium (RA). The study was approved by the Institutional Animal Care and Use Committee of Columbia University.

B. Clinical study

For the clinical study, eight patients (61.1±15.1 years old) underwent AF ablation, during which ICE was routinely used as a component of their procedure. The ICE catheter was inserted into the femoral vein and advanced under direct fluoroscopic guidance as per standard protocol to the right atrium. B-mode images of the right and left atrium with the

ablation catheter in the ultrasound view were recorded. Ultrasound data were acquired before and/or during and/or after ablation in similar echocardiographic views and similar heart rhythm (Table 1). Two patients (Patient #1 and Patient #2) were investigated to carry out a reproducibility study. The number of patients for which data were acquired both before and after ablation was N = 3 (Patient #3, Patient #4 and Patient #5). The number of patients for which data were acquired both before and during ablation was N = 2 (Patient #3 and Patient #6). The number of patients for which data were acquired after ablation at different times was N = 3 (Patient #4, Patient #6 and Patient #7). The number of patients for which data were acquired both during and after ablation was N = 1 (Patient #8). RF ablation was either performed around the pulmonary veins, and/or cavotricuspid isthmus (CTI) and/or left atrium (LA). The study protocol was approved by an Institutional Review Board of Columbia University and informed consent was obtained prior to the study.

C. Ultrasound acquisition

A 5.8-MHz ICE catheter with 64 elements and 13 mm active aperture (ViewFlex PLUS ICE catheter, St. Jude Medical, St. Paul, MN, USA) on an ultrasound system (Viewmate Z, St. Jude Medical, St. Paul, MN, USA) was used. The imaging depth was set to 90 mm to be able to image at least one heart chamber such as the left atrium. The ultrasound system was connected to a computer via a serial cable (Figure 1) which allowed control over the parameters and the acquisition as well as data transfer to a hard drive connected to the system [34]. High frame rate imaging was achieved by reconstructing the entire frame from a single beam transmit. An unfocused diverging beam transmit was used in order to achieve a frame rate of 1200 fps which was the highest frame rate achievable by this scanner at a depth of 90 mm (Figure 2). In order to send an unfocused beam with a diverging angle of 90°, a virtual source was placed 6.5 mm behind the transducer which corresponds to half the size of the active aperture. The virtual source was centered relative to the transducer. The distance between the virtual source and each element of the transducer was computed in order to obtain the time delay to apply to each element to obtain a diverging wave. The 24 central elements had no apodization whereas the remaining 20 elements on each side had a weak apodization in transmit. Prior to *in vivo* application, the transmitted unfocused beam was characterized with a hydrophone (HGL-0200, ONDA, Sunnyvale, CA, USA) in a water-filled tank. The hydrophone was set on a mechanical stage and the probe was attached to the wall of the tank. The hydrophone was moved along the lateral direction at three different axial depths (2mm, 50mm and 90mm) and the maximum pressure was obtained for each lateral position.

Echocardiographic views of LA were acquired for the canine study while views of LA as well as RA and right ventricle (RV) in the region of the CTI were acquired in humans.

The In-phase/Quadrature (IQ) data were acquired on all the 64 channels in parallel and stored in the system buffer (Figure 3). At 90-mm depth and 1200 fps, the buffer of the ultrasound system could store up to 620 ms of IQ signals. Conventional B-mode images were acquired at 35 fps at the same location to help for structure identification. The data were transferred to a computer for off-line processing.

D. RF signals reconstruction

The RF signals were obtained from the IQ data and upsampled to 50 MHz to increase the quality of the motion estimation. The RF signals were then reconstructed using a standard delay-and-sum algorithm described as follows. A grid of points onto which the RF signals would be reconstructed was defined in a polar coordinate system on a region of 90° field of view with 128 lines and depth of 90 mm with a radial grid step of 15.4 μm and which origin was the virtual source. The time of flight T_f between the emission from the transducer and the reception on all the elements of the signals from every points of the grid was computed as:

$$T_f = T_t + T_r - T_d + T_b \quad (1)$$

where

$$T_t = \frac{\sqrt{x^2 + z^2}}{c} \quad (2)$$

is the time of flight from the virtual source to a point of the grid located at (x,z) and c is the speed of sound assumed to be 1540 $m.s^{-1}$.

$$T_r = \frac{\sqrt{(x - x_i)^2 + (z - z_f)^2}}{c} \quad (3)$$

is the time of flight from the pixel located at *(x,z)* to the i^{th} element of the transducer located at (x_i,z_f)

$$T_d = \frac{z_f}{c} \quad (4)$$

is the time that needs to be removed from T_f to take into account the beginning of acquisition when emitted from the center element located at $(0,z_f)$ and T_b takes into account a bulk delay related to the ultrasound system and the propagation in the lens at the surface of the transducer (Figure 2). The amplitude of each RF channel signal at each point of the grid was then computed using 1-D linear interpolation. Receive focusing at each point of the grid was performed by summing the interpolated amplitude of the RF channel signals across all the elements of the transducer. The reconstruction operation was performed on a GPU (Tesla C2075, NVIDIA, Santa Clara, CA) in order to increase the computation speed. A B-mode image was obtained (Figure 4) from the reconstructed RF data by a Hilbert transform and a manual segmentation was performed to retrieve the myocardium. The conventional B-mode provided landmarks to assist the myocardial segmentation. The contrast-to-noise ratio (CNR) was computed for both the reconstructed B-mode obtained from the diverging wave transmit and for the conventional B-mode for approximately the same view and same phase of the cardiac cycle. The CNR was defined as follows [35]

$$CNR = \frac{2(\mu_t - \mu_b)^2}{\sigma_t^2 + \sigma_b^2}$$

where μ_t and μ_b are the mean of the amplitude inside the region of interest corresponding to the tissue and to the background respectively and σ_t and $\sigma_b$are the standard deviation of the amplitude inside the region of interest corresponding to the tissue and to the background respectively.

E. Displacement and strain estimation

The displacement between two successive frames was estimated by normalized 1-D cross-correlation [36] with a window length of 10 wavelengths (2.7mm) as suggested by Chen et al. [37] and 95% overlap. The displacements were then integrated during atrial emptying (passive and active) to obtain the cumulative displacements. The relative myocardial wall displacement was therefore used as a surrogate to determine the emptying phase. During emptying of a heart chamber, its volume decreases. Displacement images obtained at high temporal resolution allow for identifying the beginning and the end of the inward motion. For LA imaging, the phase from maximal size to minimal size of the LA includes both LA conduit (passive emptying) and contractile (active emptying) function. Although out-of-plane motion can affect the apparent size of the LA in the echocardiographic view, the LA maximum volume corresponds to the beginning of LA conduit and LA minimum volume corresponds to the end of LA active emptying [38, 39]. The patients for which no clear inward motion was observed were discarded from the study. End-emptying atrial strain was defined as the strain accumulated from the beginning to the end of the atrial inward motion. Previous studies recommended defining end-diastole (systole) as the frame in the cardiac cycle in which the cardiac dimension is the largest (smallest) [40]. The selection of the frames corresponding to emptying was performed using similar criteria such as myocardial wall relative displacement for the ablation and the non-ablation cases. For RA and RV imaging, the closure of the tricuspid valve was used as a reference for the phase selection. Cumulative axial strains were computed from cumulative axial displacements by applying a least-squares estimator [41] with a kernel equal to 2mm using a Savitzky-Golay filter [42] in order to decrease the noise amplification due to gradient operation.

A region of interest of approximately the same size and location was selected in the lateral wall of each canine LA to compute the value of the cumulative axial strain at end atrial emptying. In order to compare before, during and after ablation in patients, strains were estimated approximately at the same location and approximately the same phase of the cardiac cycle and during the same rhythm (normal sinus rhythm, AF or atrial flutter) in a region of interest of approximately 5×5 mm^2. The size of the region of interest was chosen to be slightly larger than the size of the tip of the ablation catheter due to heat diffusion as well as catheter movement during the ablation. Mean and standard deviation of the strain in the selected region of interest were computed. For the dog results or when comparing different groups (before, during and after), the mean and standard deviation reported are computed across the different individuals in the group.

In order to investigate the reproducibility of our technique, ultrasound data were acquired twice with approximately one minute between each acquisition in the same echocardiographic view without moving the ICE catheter in two patients. For one patient, the LA was imaged whereas for the other patient the RA and RV were imaged. In all the

cases, the ultrasound data were acquired before ablation and during sinus rhythm. End-emptying atrial strain were imaged and compared for both acquisitions in each patient.

RESULTS

Myocardial displacement and strain were imaged with ICE at 1200 fps using parallel beamforming in three canines and eight humans *in vivo*. The acquisition duration was less than the duration of a cardiac cycle. For each acquisition either the entire emptying or filling phase could be obtained, but not both. The acquisition duration was also less than the duration of the ablation at a specific location which hindered to demonstrate the evolution of the strain as a function of ablation time. The ultrasound data were acquired during normal sinus rhythm, AF or atrial flutter. Conventional B-mode images were also acquired to assist myocardial segmentation. The CNR was computed for both the reconstructed B-mode obtained from a diverging wave imaging and for a conventional B-mode. The CNR for the reconstructed and the conventional B-mode was 5.1 and 9.3 respectively.

A. Canine study

Axial displacement and strain were assessed in the LA from ICE acquisitions in LA short axis view of three canines during atrial emptying (Figure 5). The ICE probe is located in the RA and oriented towards the LA. Axial displacements are shown at the end of LA emptying in Figure 5.A-C. Displacements in the lateral (anatomical) direction are in blue whereas displacements in the medial direction are in red. The interatrial septum wall is detected moving in the lateral direction (blue) whereas the left lateral wall is moving in the medial direction (red). A schematic indicating the LA wall displacements is shown in Figure 5.G. The corresponding strains (Figure 5.D-F) show that positive strain in red (radial thickening) is observed in the lateral wall and the interatrial septum whereas negative strain in blue (circumferential shortening) occurs in the anterior and posterior walls. Similar displacement and strain patterns are observed for the three canines. The mean absolute axial cumulative strain at the atrial emptying phase in the selected region of interest in the lateral wall across the three dogs was 15.8±12.1% where 12.1% reflects the variability across the three dogs.

B. Clinical study

The reproducibility of our technique was investigated in two patients before ablation in sinus rhythm. End atrial emptying strains for two consecutive acquisitions in two different patients are show in Figure 6. End LA emptying strain is shown for two consecutive acquisitions in Patient #1 (Figure 6.A and 5.B). End RA emptying strain is show for two consecutive acquisitions in Patient #2 (Figure 6.D and 5.E). A similar strain pattern is obtained for both acquisitions in each patient.

Displacements and strains were also estimated in the LA of AF patients before, during and after an RF ablation procedure. Cumulative axial displacement before ablation at end LA emptying for Patient #4 during atrial fibrillation is shown in Figure 7.A. The ICE probe is located in the RA and oriented towards the LA. During LA emptying, LA contracted inwards (Figure 7.E). The corresponding strains at end LA emptying are shown in Figure 7.B. In this view, radial thickening is observed in the anterior wall and end LA emptying

absolute strain magnitude reached approximately 16.4±10.1%. Axial displacements during ablation in the LA of the same patient and for approximately the same cardiac phase and rhythm are shown in Figure 7.C. LA contracted inwards. The corresponding strains are shown in Figure 7.D. The black ellipse indicates the region of ablation and the red arrow points to the ablation catheter. The absolute strain magnitude is lower, approximately 0.9±3.0%, in the region where ablation occurred which is less than prior to ablation. The decrease in strain was observed in the region of ablation whereas the regions where no ablation was performed did not exhibit a significant change in strain. This decrease in strain indicates that the contractility of the myocardium is reduced in the ablated region which indicates lesion formation.

Cumulative axial displacements and strains at RA end-emptying were also evaluated in the CTI region of Patient #6 in sinus rhythm during and after RF ablation in this region (Figure 8). The ICE probe is located in the RA and oriented towards the right ventricle (RV). Axial displacements in the patient RA and RV during ablation are shown in Figure 8.A. The RA and RV lateral walls moved in the superior direction (Figure 8.E). The corresponding strains are shown in Figure 8.B. In this view, RA longitudinal shortening and RV longitudinal lengthening are shown in their respective lateral walls. The absolute strain magnitude in the RA lateral wall was approximately 43.0±18.1%. Axial displacements in the same patient RA and RV in the CTI region after ablation and during approximately the same cardiac phase are shown in Figure 8.C. The RA and RV lateral walls moved in the superior direction. The corresponding strain is shown in Figure 8.D and was approximately 33.7±15.8% in the region of ablation which is less than prior to ablation. Moreover, the strain magnitude in the ablated region was decreased on the endocardial side of the myocardium more than on the epicardial side which suggests that the transmurality of the lesion can be imaged with this method.

The strain variation at the different stages of the ablation for all patients is shown in Figure 9. Error bars represent standard deviation in the selected region of interest corresponding to the region of ablation. Strain was compared before and after ablation for three patients totaling four ultrasound views. Two ultrasound views were obtained for one of the three patients. The average absolute strain magnitude before ablation was 17.4±9.3% and decreased to 6.7±3.1% after ablation. Strain was also compared before and during ablation for two patients with one ultrasound view per patient. The average absolute strain magnitude was 11.3±7.2% before ablation and 4.0±4.4% during ablation. Strain after ablation at a certain time ($\mathcal{E}^{t}$) was also compared to strain after ablation later on ($\mathcal{E}^{t+\Delta t}$). The average absolute strain magnitude was 16.2±17.7% ablation at time t and 10.9±10.7% after ablation at time $t+\Delta t$.

DISCUSSION

Being able to characterize thermal lesions created by radio-frequency (RF) ablation of the heart is of paramount interest to enable real time assessment of lesions allowing for characterization of transmurality and gaps which in turn may aid in long term success of ablation procedure. Myocardial Elastography (ME) is an ultrasound technique that, combined with intracardiac echocardiography (ICE) can provide information on the

mechanical properties of tissues. The aim of this study was two-fold: (1) use diverging wave imaging and parallel beamforming with ICE to image myocardial strain at high temporal resolution during atrial emptying in canines and humans *in vivo* and (2) investigating the difference in myocardial strains with ICE before, during and after radio-frequency ablation during a clinical ablation procedure. The performance of diverging wave imaging was compared to that of conventional B-mode imaging by comparing the contrast-to-noise ratio (CNR) for both cases. The CNR was found to be 5.1 for the reconstructed B-mode and 9.3 for the conventional B-mode. A better contrast is obtained for the conventional B-mode due to focused transmit for each line which gives a better lateral resolution. However, theacquisition of RF channel data for diverging wave imaging allows for a better temporal resolution compared to conventional B-mode imaging and several studies have shown that RF signals provide significant performance advantages over envelope signals [43-45]. A preliminary feasibility study was conducted on three normal canines to show the feasibility of imaging axial strain with ICE at high frame rate using diverging waves and to assess the performance of the ME method with ICE. Eight patients undergoing RF ablation which required use of ICE during ablation delivery in their left atrium and cavotricuspid isthmus (CTI) were then investigated to show the initial feasibility of clinical application of the technique. This method can be of a significant interest for the assessment of lesion location induced by RF ablation during the ablation procedure to ensure the efficiency of electrical isolation and conduction block to treat the arrhythmia as mechanical contraction at a region of the myocardium follows electrical activation of the same region [46].

A. Canine study

In the canine study, ME was performed in the LA of three normal canines (Figure 3). Axial displacements and strains were accumulated during LA emptying. The orientation of the ICE transducer relative to LA chamber allowed estimation mainly in the radial (in septum and lateral regions) and circumferential (in anterior and posterior regions) directions. Strains at end LA emptying indicated radial thickening (red) in the lateral wall and the interatrial septum whereas circumferential shortening (blue) occurred in anterior and posterior region. This was consistent with the LA displacement which showed that the interatrial septum wall moved in the lateral direction (blue) whereas the left lateral wall moved in the medial direction (red). Similar axial strain pattern were found in the three dogs. These preliminary findings point to the potential of ME to be combined with ICE in order to pinpoint successful delivery of ablation lesions as demarcated by changes in tissue mechanics after ablation.

B. Clinical study

The reproducibility of our technique was investigated in two patients before ablation in sinus rhythm. Similar end atrial emptying strain were obtained for two consecutive acquisitions in each patient which indicates a good reproducibility of axial strain imaging using diverging wave with ICE. Feasibility was afterwards tested in a clinical study, in which AF patients underwent ICE before, during and after RF ablation. Axial displacements and strains were obtained during LA or RA emptying. The average absolute value of strain at end atrial emptying was found to be lower after ablation (6.7±3.1%) than before (17.4±9.3%) in approximately the same region. The average value of strain after ablation was 2.6 times

lower than before ablation. This decrease in strain was concluded to be due to local stiffening of the tissue caused by the thermal ablation. Also for another set of ultrasound views, average absolute value of strain at end atrial emptying was found to be lower during ablation (4.0±4.4%) than before (11.3±7.2%) in approximately the same region. The average value of strain during ablation was 2.8 times lower than before ablation. For another set of ultrasound views, strain after ablation at a certain time was also compared to strain after ablation later on following with several ablations in between. The average absolute strain magnitude was 16.2±17.7% after ablation and 10.9±10.7% later on after ablation. The average value of strain after ablation at time $t+\Delta t$ was 1.5 times lower than after ablation at time t.

Similarly, cumulative axial displacements and strains were obtained in the RA and RV regions during RA emptying during and after CTI ablation (Figure 8). In this view, only longitudinal displacements and strains in the lateral wall could be estimated. At end atrial emptying, the RA and RV lateral walls moved in the superior direction. End-emptying atrial absolute strain was 43.0±18.1% during ablation and 33.7±15.8% after ablation.

In this study, for the first time to the authors knowledge the feasibility of myocardial strain estimation using RF signals at high temporal resolution and high line density with ICE during a clinical ablation procedure was shown. High temporal resolution entails good motion estimation and thus good strain quality as it is less subjected to decorrelation [47, 48]. Atrial strain imaging can be used to characterize the mechanical properties of the atria transmurally as well as along the myocardium. This is of key interest in order to assess the efficacy of lesions to inhibit conduction as conduction recovery was shown to be related to the non-transmurality and gap between lesions generated during ablation. In particular, the RF ablation procedure of AF although usually initiated with pulmonary vein isolation can also include targeted sites for linear ablation such as the LA roof, the anterior and posterior walls or CTI in RA [3]. Thus, being able to characterize thermal lesions in these regions would improve the assessment of efficacy of lesion delivery. In this study, we have shown that strain can be estimated in LA and RA during ablation. This study also shows that this technique can be applied to image the heart in different cardiac rhythms as images were taken in normal sinus rhythm, AF and atrial flutter. We observed a decrease in strain during and after ablation in the LA and the RA which indicates a change in tissue mechanics. Several studies have investigated the effect of ablation on LA contractility. Boyd et al. reported that LA strain during atrial relaxation and strain rate during atrial contraction were lower in patients who underwent RF ablation of AF and maintained sinus rhythm for 6 months follow-up than normal controls [18]. The global left atrial strain in patients who underwent RF ablation was 2.4 times lower than in normal controls. Although not expressing the same quantity as the ratio calculated in this study, this ratio reflects a change of mechanical properties due to ablation and was found to be in the same order of magnitude as what was found in this study. They attributed this observation to atrial scarring and loss of atrial myocardial mass. Schneider et al. observed on the other hand that patients who remained in sinus rhythm three months after RF ablation of AF had increased strain in LA during emptying and diastole whereas patient who had recurrent AF after three months tended to have decreased strain in LA compared to before ablation [49]. However, in these

previous studies, atrial function in ablated patients was measured after several months follow-up whereas in this study strains are measured several minutes to hours before, during and after ablation. Eyerly et al. investigated the change of acoustic radiation force induced displacement of myocardial tissue with ICE in canines during an RF ablation [24, 50]. They reported that displacements in ablated sites were inferior to displacement in unablated sites. The ARFI-induced displacements in ablated sites were 1.9 times lower than in unablated sites. They attributed this change to lesion formation, observed in tissue pathology, caused by RF ablation. This is consistent with our results showing a decrease of strain in the RF ablated region. These results suggest that ME when fully integrated with ICE can be used to guide the ablation by ascertaining myocardium mechanics as a surrogate for adequate ablation delivery.

Limitations

The study has several limitations that can be overcome in the future. As mentioned previously, the identification of the emptying phase was obtained from the myocardial walls relative displacements and not from the ECG signal. Despite high temporal resolution of displacement data and due to manual selection, the phase of the cardiac cycle may not be perfectly matched for the different cases before, during and after ablation in a moving heart. The inward motion was not as clear during AF as during sinus rhythm indicating thus that AF can induce additional errors in the selection of the cardiac phase. The cardiac phase identification would be more accurate and consistent with ECG than with assessment of wall displacement. Because the phase selection was performed from the beginning to the end of the LA inward motion, the relative contribution of LA conduit and contractile function to end-emptying atrial strain and to the change in strain was not assessed. The synchronous acquisition and storage of the ECG with RF data was not implemented for the purposes of this study but is ongoing.

The selection of the same region of interest before, during and after ablation on the diverging wave images and on the B-mode images was performed manually by visually identifying landmarks such as the position of heart valve. Despite the efforts made to obtain similar ultrasound views before, during and after ablation on the diverging wave images and on the B-mode images there could be a mismatch on the selected region of interest. This could explain why the strain is slightly higher during ablation than before ablation for patient #3. Since only the axial component is estimated, this technique is angle-dependent [51, 52]. However, the comparison in strain was performed before, during and after ablation on the selected ROIs. The average value of strain after ablation was 2.6 times lower than before ablation. This change in strain is mainly due to the ablation than to the error due to not perfectly matched ROIs. If different ROIs are compared, different strain value will be obtained both due to a strain inhomogeneity inherent to the mechanical properties of the tissue and to the angle-dependency. The strain value can therefore be under- or overestimated based on the inherent strain distribution in the tissue and on insonification angle relative to the orientation of the myocardial wall. Also, radial thickening, circumferential and longitudinal shortening occur during atrial systole. Therefore, if the axial direction is mainly aligned with the radial direction, positive strain will be obtained whereas negative strain will be obtained if the axial direction is mainly aligned with the

circumferential or longitudinal direction. It has to be noted that angle-independency can be achieved by estimating the lateral displacement and strain and therefore derive the angle-independent radial and circumferential strain [29]. However, this goes beyond the scope of this study. In this study, high frame rate was obtained with parallel beamforming using a diverging wave transmit sequence. One frame was obtained from a single firing and yielded a poor lateral resolution. Spatial compounding of diverging waves can be used to increase the lateral resolution but at the cost of decreasing the frame rate which would entail more decorrelation. The trade-off between compounding and frame rate in order to obtain the best elastographic signal-to-noise ratio is currently under investigation.

The pressure profile was measured in the lateral direction at 90mm axial depth indicates a beamwidth of approximately 35 mm at −6dB (Figure 10). The transmit sequence was currently not fully optimized and yielded a transmit beam with a relatively weak divergence due to an apodization on the lateral elements of the transducer. Modifications of the transmit sequence are currently being performed. These improvements should entail more accurate motion estimation on the outer regions.

Finally, this study was performed in three canines without RF ablation and eight humans *in vivo* during a clinical RF ablation procedure. The results presented here demonstrate the clinical feasibility of incorporating this imaging modality into everyday practice. Further studies will be needed to include a higher number of patients to further assess the performance of the method and also to assess the applicability of this imaging technique in other chambers of the heart such as the right and left ventricle during VT ablation. An ablation study on canine has also to be performed to investigate the relationship between mechanical properties of the myocardium in ablated regions and lesion features that can be obtained with histology.

CONCLUSIONS

This preliminary feasibility study demonstrated that myocardial strains can be imaged with ICE at high temporal and high line density in canines and humans *in vivo*. The ablated regions in the human myocardium were shown to have lower strains than before ablation. Some improvements are currently being developed to obtain a more accurate myocardial strain characterization. Myocardial elastography applied intracardially can be used to visualize thermal lesions during RF ablation.

ACKNOWLEDGEMENTS

This work was supported by NIH R01-EB006042 and R01-HL114358. The authors would like to thank Seshadri Srinivasan from Zonare Medical Systems for his involvement in writing the transmit sequence for the ultrasound system. The authors also thank Stanley Okrasinski, Alexandre Costet, and Ethan Bunting from the Department of Biomedical Engineering for their helpful comments and all the members of the Electrophysiology lab for their help during the clinical study.

REFERENCES

[1]. Go AS, et al. Prevalence of diagnosed atrial fibrillation in adults: national implications for rhythm management and stroke prevention: the AnTicoagulation and Risk Factors in Atrial Fibrillation (ATRIA) Study. JAMA. May 9.2001 285:2370–5. [PubMed: 11343485]

[2]. Miyasaka Y, et al. Secular trends in incidence of atrial fibrillation in Olmsted County, Minnesota, 1980 to 2000, and implications on the projections for future prevalence. Circulation. Jul 11.2006 114:119–25. [PubMed: 16818816]

[3]. Huang, SKS.; Wood, MA. Catheter Ablation of Cardiac Arrhythmias. 2nd. Saunders Elsevier; Philadelphia: 2011.

[4]. Cappato R, et al. Prospective assessment of late conduction recurrence across radiofrequency lesions producing electrical disconnection at the pulmonary vein ostium in patients with atrial fibrillation. Circulation. Sep 30.2003 108:1599–604. [PubMed: 12963643]

[5]. Melby SJ, et al. Atrial fibrillation propagates through gaps in ablation lines: implications for ablative treatment of atrial fibrillation. Heart Rhythm. Sep.2008 5:1296–301. [PubMed: 18774106]

[6]. Miller MA, et al. Acute electrical isolation is a necessary but insufficient endpoint for achieving durable PV isolation: the importance of closing the visual gap. Europace. May.2012 14:653–60. [PubMed: 22417723]

[7]. Shah DC, et al. Area under the real-time contact force curve (force-time integral) predicts radiofrequency lesion size in an in vitro contractile model. J Cardiovasc Electrophysiol. Sep.2010 21:1038–43. [PubMed: 20367658]

[8]. Avitall B, et al. The effects of electrode-tissue contact on radiofrequency lesion generation. Pacing Clin Electrophysiol. Dec.1997 20:2899–910. [PubMed: 9455749]

[9]. Nath S, Haines DE. Biophysics and pathology of catheter energy delivery systems. Prog Cardiovasc Dis. Jan-Feb;1995 37:185–204. [PubMed: 7831466]

[10]. Skrumeda LL, Mehra R. Comparison of standard and irrigated radiofrequency ablation in the canine ventricle. J Cardiovasc Electrophysiol. Nov.1998 9:1196–205. [PubMed: 9835264]

[11]. Slabaugh TK, et al. Monitoring radiofrequency renal lesions in real time using contrast-enhanced ultrasonography: a porcine model. J Endourol. Jun.2005 19:579–83. [PubMed: 15989450]

[12]. Solbiati L, et al. Monitoring RF ablation. Eur Radiol. Oct; 2004 14(Suppl 8):P34–42. [PubMed: 15700331]

[13]. Pareek G, et al. Elastographic measurements of in-vivo radiofrequency ablation lesions of the kidney. J Endourol. Nov.2006 20:959–64. [PubMed: 17144871]

[14]. Doi A, et al. Real time quantification of low temperature radiofrequency ablation lesion size using phased array intracardiac echocardiography in the canine model: comparison of two dimensional images with pathological lesion characteristics. Heart. 2003; 89:923–927. [PubMed: 12860873]

[15]. Podrid, PJ.; Kowey, PR. Cardiac Arrhythmia: Mechanisms, Diagnosis and Management. 2nd. Lippincott Williams and Wilkins; Philadelphia: 2001.

[16]. Kiss MZ, et al. Viscoelastic characterization of in vitro canine tissue. Phys Med Biol. 2004; 49:4207–4218. [PubMed: 15509061]

[17]. Pernot, M., et al. Mapping myocardial elasticity changes after RF-ablation using supersonic shear imaging; Computers in Cardiology, 2009; 2009. p. 793-796.

[18]. Boyd AC, et al. Differential recovery of regional atrial contraction after restoration of sinus rhythm after intraoperative linear radiofrequency ablation for atrial fibrillation. Am J Cardiol. Feb 15.2009 103:528–34. [PubMed: 19195515]

[19]. Thomas SP, et al. Effect of atrial radiofrequency ablation designed to cure atrial fibrillation on atrial mechanical function. J Cardiovasc Electrophysiol. Jan.2000 11:77–82. [PubMed: 10695466]

[20]. Wang J, et al. Analysis of postsystolic myocardial thickening work in selective myocardial layers during progressive myocardial ischemia. J Am Soc Echocardiogr. Sep.2006 19:1102–11. [PubMed: 16950464]

[21]. Stephens DN, et al. Multifunctional catheters combining intracardiac ultrasound imaging and electrophysiology sensing. IEEE Trans Ultrason Ferroelectr Freq Control. Jul.2008 55:1570–81. [PubMed: 18986948]

[22]. Yue Y, et al. Speckle tracking in intracardiac echocardiography for the assessment of myocardial deformation. IEEE Trans Biomed Eng. Feb.2009 56:416–25. [PubMed: 19272903]

[23]. Hollender PJ, et al. Intracardiac echocardiography measurement of dynamic myocardial stiffness with shear wave velocimetry. Ultrasound Med Biol. Jul.2012 38:1271–83. [PubMed: 22579544]

[24]. Eyerly SA, et al. Intracardiac acoustic radiation force impulse imaging: a novel imaging method for intraprocedural evaluation of radiofrequency ablation lesions. Heart Rhythm. Nov.2012 9:1855–62. [PubMed: 22772134]

[25]. Eyerly SA, et al. An in vitro assessment of acoustic radiation force impulse imaging for visualizing cardiac radiofrequency ablation lesions. J Cardiovasc Electrophysiol. May.2010 21:557–63. [PubMed: 20021518]

[26]. Montserrat S, et al. Left atrial deformation predicts success of first and second percutaneous atrial fibrillation ablation. Heart Rhythm. Aug 27.2014

[27]. Motoki H, et al. Global Left Atrial Strain in the Prediction of Sinus Rhythm Maintenance after Catheter Ablation for Atrial Fibrillation. J Am Soc Echocardiogr. Sep 23.2014

[28]. Spethmann S, et al. Left atrial mechanics predict the success of pulmonary vein isolation in patients with atrial fibrillation. J Interv Card Electrophysiol. Jun.2014 40:53–62. [PubMed: 24535682]

[29]. Lee WN, et al. In vivo study of myocardial elastography under graded ischemia conditions. Phys Med Biol. Feb 21.2011 56:1155–72. [PubMed: 21285479]

[30]. Shougang W, et al. A composite high-frame-rate system for clinical cardiovascular imaging. Ultrasonics, Ferroelectrics and Frequency Control, IEEE Transactions on. 2008; 55:2221–2233.

[31]. Montaldo G, et al. Coherent plane-wave compounding for very high frame rate ultrasonography and transient elastography. IEEE Trans Ultrason Ferroelectr Freq Control. Mar.2009 56:489–506. [PubMed: 19411209]

[32]. Hasegawa H, Kanai H. High-frame-rate echocardiography using diverging transmit beams and parallel receive beamforming. Journal of Medical Ultrasonics. 2011; 38:129–140. 2011/07/01.

[33]. Provost J, et al. Electromechanical wave imaging for arrhythmias. Phys Med Biol. Nov 21.2011 56:L1–11. [PubMed: 22024555]

[34]. Mo, L., et al. Compact ultrasound scanner with simultaneous parallel channel data acquisition capabilities; Ultrasonics Symposium, 2008. IUS 2008. IEEE; 2008. p. 1342-1345.

[35]. Thitaikumar A, et al. Signal-to-noise ratio, contrast-to-noise ratio and their trade-offs with resolution in axial-shear strain elastography. Phys Med Biol. Jan 7.2007 52:13–28. [PubMed: 17183125]

[36]. Luo J, Konofagou E. A fast normalized cross-correlation calculation method for motion estimation. IEEE Trans Ultrason Ferroelectr Freq Control. Jun.2010 57:1347–57. [PubMed: 20529710]

[37]. Chen H, et al. Improvement of elastographic displacement estimation using a two-step cross-correlation method. Ultrasound Med Biol. Jan.2007 33:48–56. [PubMed: 17189046]

[38]. Abhayaratna WP, et al. Left atrial reservoir function as a potent marker for first atrial fibrillation or flutter in persons > or = 65 years of age. Am J Cardiol. Jun 1.2008 101:1626–9. [PubMed: 18489941]

[39]. Trikas A, et al. Relation of left atrial volume and systolic function to the hormonal response in idiopathic dilated cardiomyopathy. Int J Cardiol. Dec.1994 47:139–43. [PubMed: 7721481]

[40]. Lang RM, et al. Recommendations for chamber quantification: a report from the American Society of Echocardiography's Guidelines and Standards Committee and the Chamber Quantification Writing Group, developed in conjunction with the European Association of Echocardiography, a branch of the European Society of Cardiology. J Am Soc Echocardiogr. Dec.2005 18:1440–63. [PubMed: 16376782]

[41]. Kallel F, Ophir J. A least-squares strain estimator for elastography. Ultrason Imaging. Jul.1997 19:195–208. [PubMed: 9447668]

[42]. Luo J, et al. Axial strain calculation using a low-pass digital differentiator in ultrasound elastography. IEEE Trans Ultrason Ferroelectr Freq Control. Sep.2004 51:1119–27. [PubMed: 15478973]

[43]. Alam SK, Ophir J. On the use of envelope and RF signal decorrelation as tissue strain estimators. Ultrasound Med Biol. 1997; 23:1427–33. [PubMed: 9428142]

[44]. Lopata RG, et al. Performance evaluation of methods for two-dimensional displacement and strain estimation using ultrasound radio frequency data. Ultrasound Med Biol. May.2009 35:796–812. [PubMed: 19282094]

[45]. Ma C, Varghese T. Comparison of cardiac displacement and strain imaging using ultrasound radiofrequency and envelope signals. Ultrasonics. Mar.2013 53:782–92. [PubMed: 23259981]

[46]. Kohl, P., et al. Cardiac mechano-electric coupling and arrhythmias. Oxford University Press; Oxford: 2011.

[47]. Chen H, et al. Ultrasound frame rate requirements for cardiac elastography: experimental and in vivo results. Ultrasonics. Jan.2009 49:98–111. [PubMed: 18657839]

[48]. Luo, J., et al. An In-Vivo Study of Frame Rate Optimization For Myocardial Elastography; IEEE Int Ultrason Symp; 2007. p. 1933-36.

[49]. Schneider C, et al. Strain rate imaging for functional quantification of the left atrium: atrial deformation predicts the maintenance of sinus rhythm after catheter ablation of atrial fibrillation. Eur Heart J. Jun.2008 29:1397–409. [PubMed: 18436560]

[50]. Eyerly SA, et al. Contrast in intracardiac acoustic radiation force impulse images of radiofrequency ablation lesions. Ultrason Imaging. Apr.2014 36:133–48. [PubMed: 24554293]

[51]. Castro PL, et al. Potential pitfalls of strain rate imaging: angle dependency. Biomed Sci Instrum. 2000; 36:197–202. [PubMed: 10834232]

[52]. Provost J, et al. Electromechanical wave imaging of normal and ischemic hearts in vivo. IEEE Trans Med Imaging. Mar.2010 29:625–35. [PubMed: 19709966]

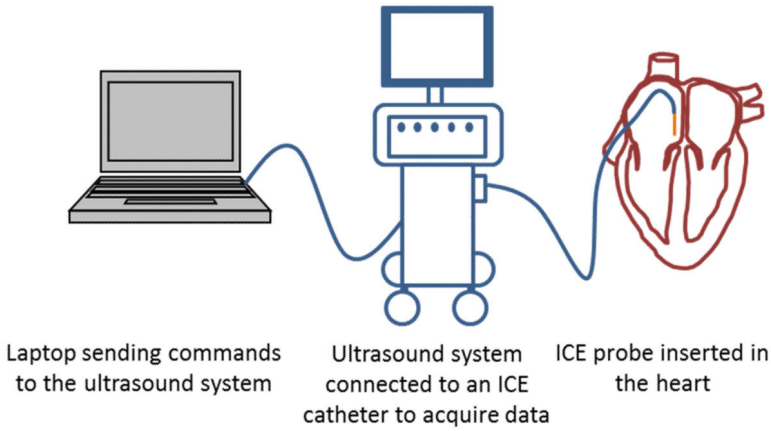

Fig. 1.

Experimental set-up. An ICE catheter connected to an ultrasound system is inserted into the right atria of canines through the jugular vein or through the femoral vein in humans. A laptop is used to send commands to the ultrasound system to set the imaging parameters, acquire and save the RF data. Media-Color 1

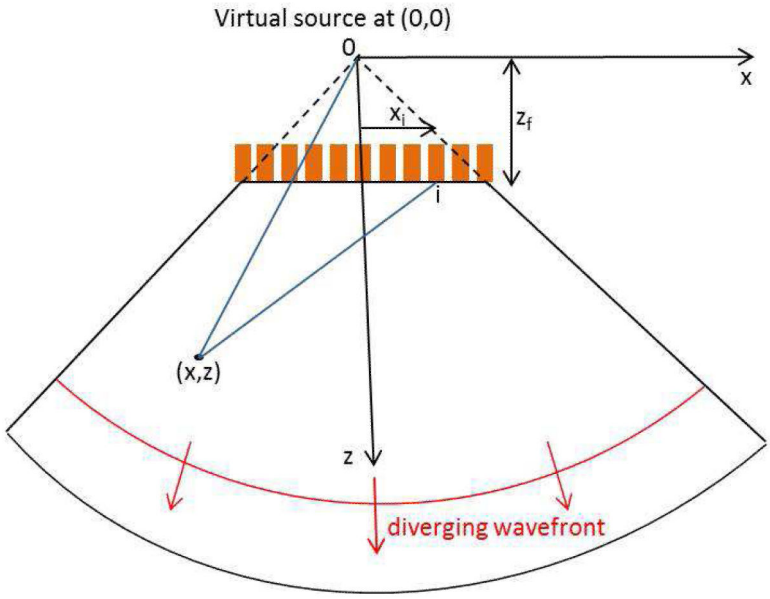

Fig. 2.

Diverging beam transmit illustration. Delays between a virtual source located at a distance z_f behind the probe and all the elements of the transducer produce a diverging beam (in red). The time of flight between the emission from the transducer and the reception on the i^{th} element located at (x_i,z_f) of the signals reflected from point of the grid located at (x,y) was computed. Media-Color 2

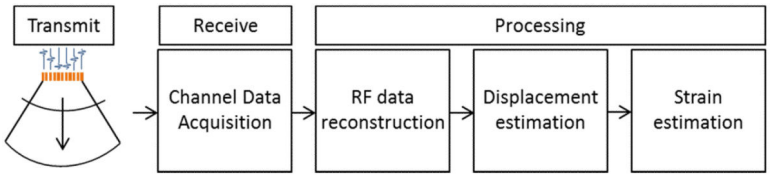

Fig. 3.

Flow chart of the acquisition and processing procedure. Delays are applied to each channel of the transducer to transmit a diverging beam. The received signals are acquired on each channel. The RF data are reconstructed using a delay-and-sum method. The RF signals are cross-correlated to estimate displacements. Strains are obtained by taking the gradient of the displacement using a least-squares estimator. Media-Color 3

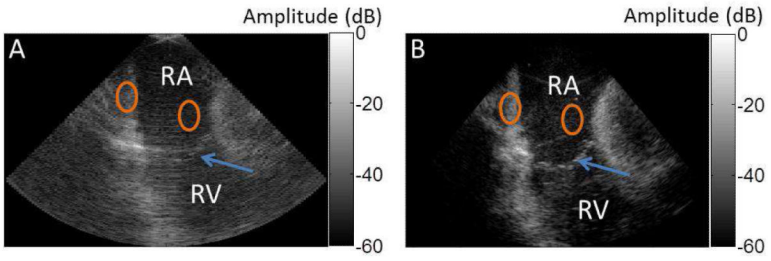

Fig. 4.

B-mode for a reconstructed image from a single diverging wave transmit (A) and for a conventional line by line acquisition (B). RA and RV denotes the right atrium and ventricle respectively. The blue arrow points to the tricuspid valve. The ellipses in orange indicate the regions chosen to compute the contrast-to-noise ratio. The ellipse on the RA wall was used for the tissue and the ellipse inside the RA cavity was used for the background. Media-Color 4

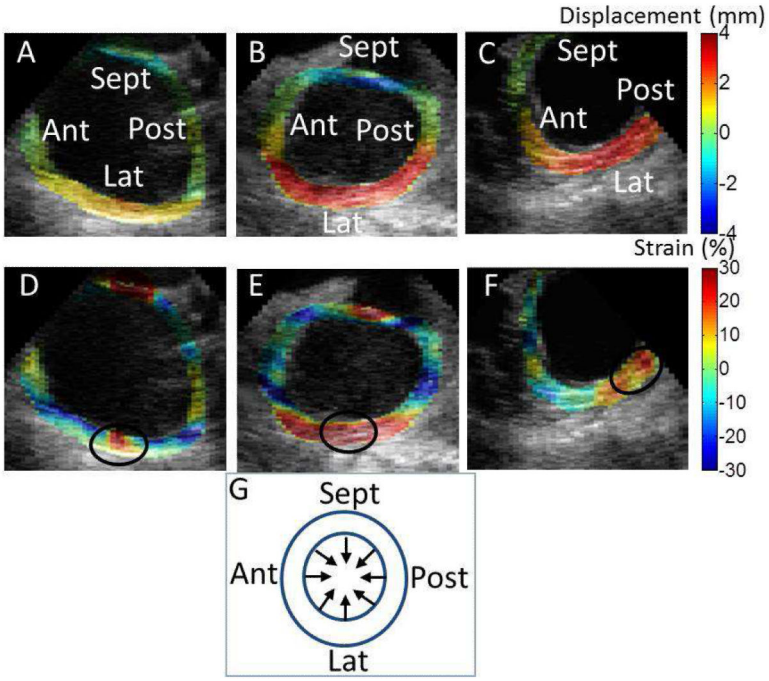

Fig. 5.

Cumulative axial displacement (A, B, C) and cumulative axial strain (D, E, F) in three canine left atrium (LA) at end LA emptying. Positive (red) displacements are in the medial direction and negative (blue) displacements in the lateral direction. The interatrial septum (Sept) wall is moving in the lateral direction whereas the left lateral (Lat) wall is moving in the medial direction. A schematic of the LA displacement is shown (G). In this view, contraction corresponds to radial thickening and circumferential shortening. Radial thickening is observed in the lateral wall and the interatrial septum whereas circumferential shortening occurs in the anterior (Ant) and posterior (Post) wall. The black ellipse indicates the region of interest for which strain were computed for comparison. Similar displacement and strain patterns are observed for the three dogs. Media-Color 5

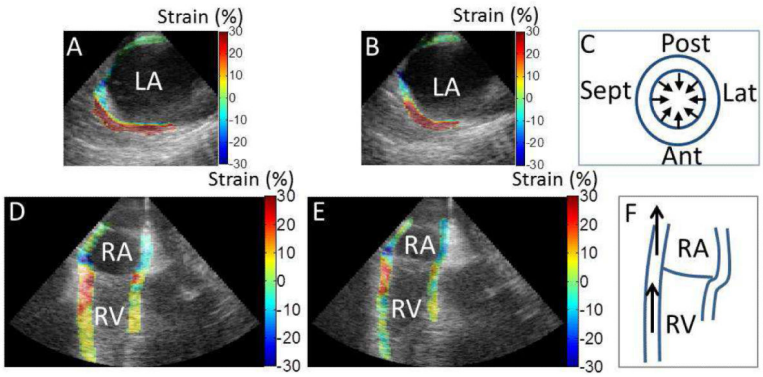

Fig. 6.

Cumulative axial strain at end LA emptying for two consecutive acquisitions in left atrium (LA) of patient #1 (A, B) and right atrium (RA) and right ventricle (RV) of patient #2 (D, E). Both patients were in sinus rhythm during both acquisitions. A schematic of the LA displacement for patient #1 (C) and of RA and RV displacement for patient #2 (F) are shown. A similar strain pattern is obtained for both acquisitions in each patient. Media-Color 6

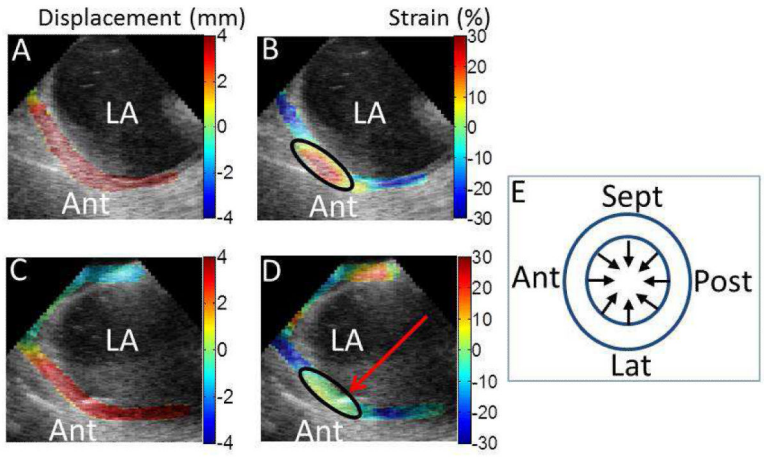

Fig. 7.

Cumulative axial displacement (A, C) and cumulative axial strain (B, D) in left atrium (LA) of an AF patient at end LA emptying. A schematic of the LA displacement is shown (E). A and B are before RF ablation whereas C and D are during. The black ellipse indicates the region of ablation and the red arrow points to the ablation catheter. The anterior (Ant) wall moved inward. Radial thickening is observed in the anterior wall and the absolute strain magnitude is approximately 15.2±9.0% before ablation and decreased to approximately 2.6±3.1% in the ablated region. Media-Color 7

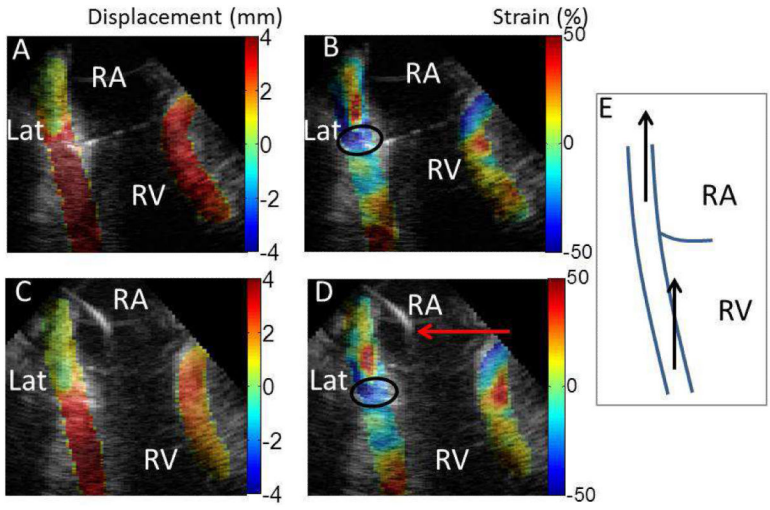

Fig. 8.

Cumulative axial displacement (A, C) and cumulative axial strain (B, D) in the right atrium (RA) and right ventricle (RV) of an AF patient at end RA emptying. A schematic of the RA and RV displacement is shown (E). A and B are during RF ablation whereas C and D are after. The black ellipse indicates the region of ablation and the red arrow points to the ablation catheter. The lateral (Lat) wall moved toward the superior direction. In this view, positive (negative) strain corresponds to longitudinal lengthening (shortening). Longitudinal shortening is observed in the RA lateral wall whereas longitudinal lengthening can be seen in the RV lateral wall. The absolute strain magnitude in RA lateral wall was approximately 44.8±15.9% during ablation and 35.1±14.5% after ablation. Media-Color 8

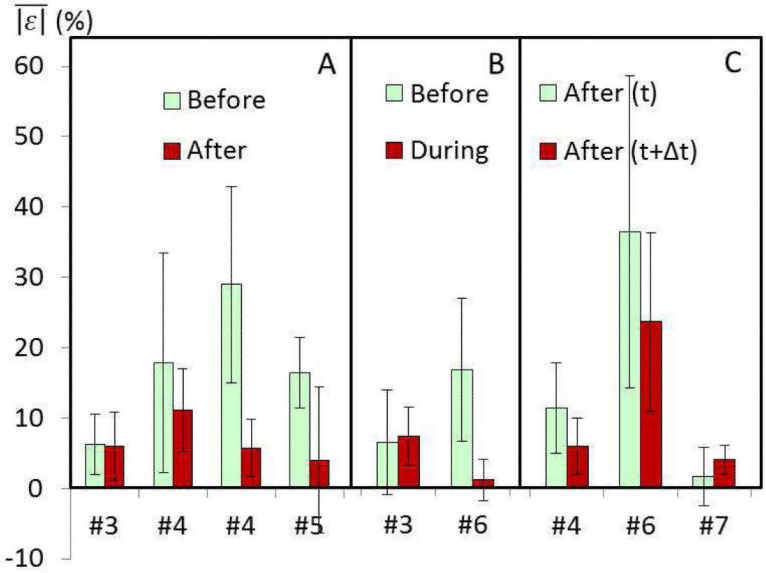

Fig. 9.

Average absolute value of strain ($|\bar{\varepsilon}|$) at end atrial emptying in the region of ablation for different patients (#). Error bars represent standard deviation in the selected region of interest corresponding to the region of ablation. Strain before and after ablation are compared for three patients totaling four different views (A). Strain before and during ablation are compared for two patients totaling two different views (B). Strain after ablation at a certain time (t) and later on a time ($t+\Delta t$) are compared for three patients totaling three different views (C). Media-Color 9

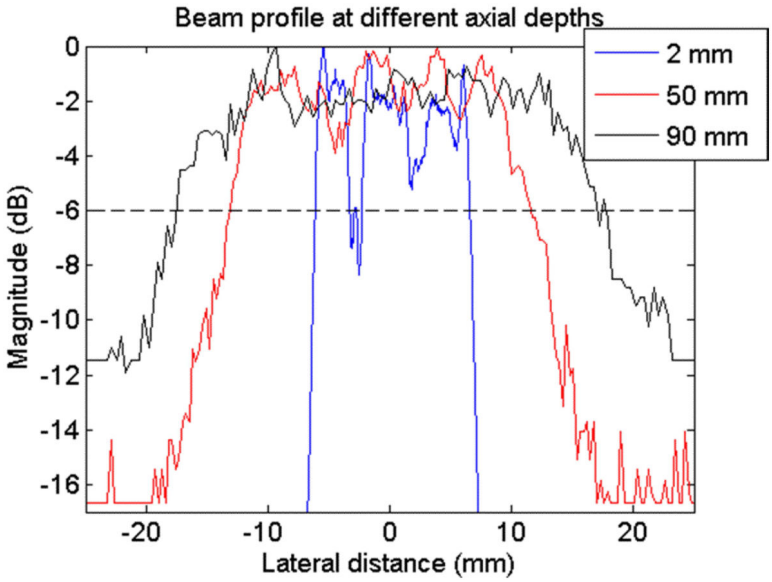

Fig. 10.

Beam profile of the ICE catheter during diverging beam transmit at 2mm (blue), 50mm (red) and 90mm (black) axial depths. The dashed line is the magnitude −6dB. Media-Color 10

Table 1

Patients scanned for different acquisitions.

Acquisition	Patients ID number
Reproducibility	#1, #2
Before and after ablation	#3, #4, #5
Before and during ablation	#3, #6
After (t) and after ($t+\Delta t$) ablation	#4, #6, #7
During and after ablation	#8